Wound-Induced Syncytia Outpace Mononucleate Neighbors during *Drosophila* Wound Repair

James S. White[1,2], Jasmine J. Su[1,4], Elizabeth M. Ruark[1], Junmin Hua[1], M. Shane Hutson[3,4*], Andrea Page-McCaw[1,2,5,6*]

***Correspondence:**

andrea.page-mccaw@vanderbilt.edu

shane.hutson@vanderbilt.edu

Author contributions: Conceptualization, J.S.W., A.P.M., M.S.H.; Formal Analysis, J.S.W., J.J.S.; Investigation, J.S.W., J.J.S., E.M.R., J.H.; Writing – Original Draft., J.S.W., A.P.M.; Visualization, J.S.W., J.J.S.; Supervision, A.P.M., M.S.H., J.S.W. ; Project Administration, J.S.W., A.P.M., M.S.H; Funding Acquisition, A.P.M., M.S.H

[1]Dept. Cell and Developmental Biology, Vanderbilt School of Medicine, Nashville, TN; [2]Program in Developmental Biology, Vanderbilt University Nashville, TN; [3]Dept. Physics and Astronomy Vanderbilt University Nashville, TN; [4]Dept. Biological Sciences, Vanderbilt University, Nashville, TN; [5]Vanderbilt-Ingram Cancer Center, Vanderbilt University, Nashville, TN; [6]Lead Contact; *Corresponding Authors

ABSTRACT:

All organisms have evolved to respond to injury. Cell behaviors like proliferation, migration, and invasion replace missing cells and close wounds. However, the role of other wound-induced cell behaviors is not understood, including the formation of syncytia (multinucleated cells). Wound-induced epithelial syncytia were first reported around puncture wounds in post-mitotic *Drosophila* epidermal tissues, but have more recently been reported in mitotically competent tissues such as the *Drosophila* pupal epidermis and zebrafish epicardium. The presence of wound-induced syncytia in mitotically active tissues suggests that syncytia offer adaptive benefits, but it is unknown what those benefits are. Here, we use *in vivo* live imaging to analyze wound-induced syncytia in mitotically competent *Drosophila* pupae. We find that almost half the epithelial cells near a wound fuse to form large syncytia. These syncytia use several routes to speed wound repair: they outpace diploid cells to complete wound closure; they reduce cell intercalation during wound closure; and they pool the resources of their component cells to concentrate them toward the wound. In addition to wound healing, these properties of syncytia are likely to contribute to their roles in development and pathology.

INTRODUCTION

Injury is a constant reality of life, and survival requires all organisms to repair wounds. Wound-induced cell behaviors like proliferation, migration, and invasion replace missing cells and close wounds [1, 2]. Other cell behaviors are induced around wounds, but their contribution to wound healing is not well understood, *e.g.*, the fusion of cells into syncytia. Syncytia are one type of polyploid cell, and it is generally appreciated that increases in ploidy – number of genomes per cell – is a common response of post-mitotic tissues and cells to injury [3-5]. Wound-induced epithelial syncytia were first observed around epidermal puncture wounds in *Drosophila* larvae and adults [3, 6], consistent with the idea of polyploidy induction in non-proliferative cells. However, recent studies have observed syncytia around wounds in mitotically competent tissues: around laser-ablation wounds in *Drosophila* pupal epidermis [7] and in zebrafish epicardium damaged by endotoxin, microdissection, or laser ablation [1]. Further, injury associated with the surgical implantation of biomaterials can cause immune cells to fuse into multinucleated giant cells, which are associated with rejection [8]. Similarly, injury induces bone marrow-derived cells to fuse with various somatic cells to promote repair [9-12]. The many instances of syncytia being induced by wounds raise the possibility that syncytia offer an adaptive benefit. It is not clear, however, what that benefit is.

Syncytia can form either by endomitosis – mitosis without cytokinesis – or by cell-cell fusion. Such fusion is widely observed throughout development in both vertebrates and invertebrates: for example myoblasts fuse into muscles [13, 14], and fusions occur in the lineages of the *C. elegans* hypodermis [15] as well as vertebrate trophoblast [16], myoblast, and osteoclast [17]. Cell fusions are also observed in disease: pathogen-induced epithelial fusion allows spreading of many viruses including human respiratory syncytial virus and SARS-CoV-2

[18]; and the fusion of cancer cells with bone-marrow derived cells is implicated in metastasis [19].

Here, we use live imaging and clonal analysis to understand the behavior of syncytia following wounding in the *Drosophila* pupal notum. The unwounded notum is a monolayer epithelium composed of mononuclear diploid cells that are mitotically competent. Nonetheless, during the first several hours after wounding, many of the surrounding cells fuse to form giant syncytia. Some fusions are obvious with apical borders breaking down, while others appear only as shrinking of a cell's apical surface. All together, fusion is a common fate of cells near wounds: about half the cells fuse to form syncytia within 70 µm of a wound with 30 µm radius. Compared to their mononuclear neighbors, syncytia have dramatically improved wound-repair abilities: they outpace smaller mononuclear cells to the leading edge, they limit the need to negotiate cell intercalations as the wound closes, and they mobilize and transport actin from distal cells to reinforce the wound margin.

RESULTS:

A mitotic tissue utilizes cell-cell fusions during wound repair.

The pupal notum is a monolayer columnar epithelium composed of diploid cells that undergo regular mitotic cycles [20] (Fig. S1A-C). To analyze cell behaviors around wounds, we live-imaged after laser ablation. Epithelial cell borders were labeled by the adherens junction protein p120ctnRFP [21] and nuclei were labeled with histone His2GFP. Two hours after wounding, we observed prominent syncytial cells around the wound (Fig.1A, Movie S1). Some syncytia appeared to contain over a dozen nuclei within epithelial borders. For both syncytial and mononuclear cells, it was difficult to assign nuclei precisely to cell borders because notum

epithelial cells are not rectangular and are not arranged at right angles with respect to the surface; in 2-D projections, a nucleus was frequently observed outside the cell's apical border (Fig. S1D). Accordingly, using apical area and nuclear density, we estimated the number of nuclei within the 3 largest syncytia in different wounds. The number of nuclei in these syncytia increased over time: at 1 h after wounding the three largest syncytia contained an average 3-13 nuclei, and 2 h after wounding they nearly doubled to 6-20 nuclei (Fig. 1B). Interestingly, larger wounds generated syncytia with larger apical areas and more nuclei, proportional to wound size, suggesting syncytium formation is a dynamic and scalable response to injury (Fig. 1 C-E).

Live imaging of cells after wounding revealed the gradual loss of p120ctn between some epithelial cells followed by syncytial rounding (Fig. 1F), suggesting epithelial cell fusion. As p120ctn was lost, the epithelial cadherin E-cadherin was also lost (Fig. S1E-H) indicating the disassembly of adherens junctions between the cells. We called this phenomenon "border breakdown". Border breakdowns were found spatially clustered in the first three to four rows of cells, 30-50 μm from the wound center, and they occurred primarily within the first hour after wounding, some within 10 minutes after wounding (Fig 1G,H). To test whether border breakdowns represented cell fusions, and not loss of adherens junctions caused by epithelial to mesenchymal transitions, we analyzed cytoplasmic mixing. Individual GFP-labeled cells were generated at random locations using the flip-out Gal4 technique [22]. Before wounding, the level of cytoplasmic GFP fluorescence was stable yet exhibited cell-to-cell variability, allowing some differentiation of cells by intensity. Minutes after a nearby laser ablation, GFP was observed to diffuse from labeled cells into neighboring unlabeled cells. GFP mixing between two cells was followed by the eventual loss of their shared p120ctn-labeled cell border, confirming that border breakdown is indeed cell fusion, but that cytoplasmic mixing occurs more than 10 minutes

before the border breakdown is first observed to start (Fig 1I, Movie S2). Border breakdowns between labeled and unlabeled cells were always preceded by GFP mixing (n=11). Thus, epithelial fusion is a rapid local response to wounding.

Cell shrinking is a second form of cell-cell fusion occurring later during wound closure.

Because border breakdowns occurred mostly within 1 h after wounding, it was unclear how syncytia grew between 1-2 h after wounding. However, an unexpected cell behavior was frequently observed during this time: the apical area of diploid epithelial cells shrank until they disappeared, which we termed “shrinking cells” (Fig. 2A). Although we first expected that shrinking cells were extruding, when we tracked the nuclei of shrinking cells, we were surprised that all nuclei moved laterally to join neighboring syncytia (n=7, Fig. 2B)), suggesting that shrinking cells are fusing cells. To better understand this behavior, we analyzed individual GFP-labeled cells. Like with border breakdowns, GFP mixing preceded the initiation of cell shrinking, although by a longer interval of one or more hours (Fig. 2C, Movie S3). Additionally, X-Z projections through GFP labeled shrinking cells are consistent with cytoplasm moving into neighboring syncytia (Fig. 2D). Shrinking cells were distributed similarly around wounds as border breakdowns but occurred later and were more numerous (Fig. 2E,F). Thus, both border breakdown and cell shrinking are indicative of cell fusion.

To determine what percentage of cells around a wound will fuse, we analyzed over 100 randomly-labeled single GFP cells within the radius of observed fusion (80 µm), tracking them for 6.5 h to assess their fate (Fig. 3A,B): a full quarter of the cells fused (25%), sharing GFP before breaking down borders or shrinking; 67% persisted as diploid cells, most with stable GFP, but infrequently (n=3) with GFP mixing and no subsequent cell fusion; the remaining 7% could

not be tracked (Fig. S2A). Fusing cells were strongly skewed toward the center of the wound: within 70 µm, about half the cells (47%) underwent fusion (Fig. 3A, right). Fusion continued for over 300 min after wounding (Fig. S2B,C) whereas border breakdown is concentrated in the first hour after wounding (Fig. 1H, Fig. S2C). Shrinking accounts for more than half of all fusing cells (Fig. 3C), and the spatial distribution of fusing cells that shrank vs. lost borders was similar (compare Figs. 1G and 2E). However, shrinking began later than border breakdowns, continued for several hours after wounding (Figs. 2F, S2C), and took longer to complete (Fig. S2D). Thus, shrinking fusion accounted for continuing syncytial growth after border breakdowns subsided. Further, cell fusion is a persistent behavior over the course of wound closure.

Syncytia outcompete mononucleate cells at the leading edge of repair.

Because about half the cells fused to form syncytia around wounds, we were able to compare the behavior of syncytial to non-syncytial cells. Comparing cell behaviors within the same wound provided a well-controlled environment for assessing how syncytia contribute to wound closure. Using live imaging, we observed that syncytia frequently overtook unfused cells as they moved toward the wound. Figure 4A shows the fusion of seven cells, with non-fusing GFP-labeled cells both distal and proximal to the fusing cells (panel 4A^{ii}, cells 1 and 4 respectively). Later the syncytium advanced beyond both unfused cells toward the wound; it even reached around and past wound-proximal cell 4 to extend the leading edge toward the wound Fig. 4A^{iii}). This behavior was evident even without GFP labeling: Fig. 4B-C show a group of cells at the leading edge of the wound, recognized by the lack of p120ctn. At 90 min after wounding, this area of the leading edge is composed of three mononuclear cells (the middle one outlined in orange and white) flanked on either side by syncytia (outlined in yellow). In

panel 4B^{iii}, both syncytia have pushed out the mononuclear cells from the leading edge. Thus, it appeared that syncytia were able to outpace mononuclear cells toward the leading edge.

Further, we noticed that by several hours after wounding, the leading edge of the wound was occupied primarily by syncytia. To investigate how syncytia came to occupy this position at the front lines of wound healing, we expressed MyoIIGFP/Zip-GFP, which along with actin forms the contractile purse string and makes the leading edge visible, along with p120ctnRFP to label cell borders. We analyzed the persistence of all mononuclear and syncytia cells at the leading edge over the course of closure for three wounds, starting when the leading edge was first visible (Fig. 4D-F). As soon as the leading edge formed 30 min after wounding, about 75% of the perimeter was occupied by syncytia (Fig. 4G); the rest of the perimeter was occupied by 10-13 small cells (Fig. 4D). As the wound closed, the syncytia became larger and displaced all the small cells, with the last small cell removed from the leading edge well before closure, which occurred 20-160 min after removal of the last small cell (Fig. 4 D,F). No small cell persisted at the leading edge through wound closure, indicating that syncytia are better able to close wounds than unfused cells.

Syncytia reduce intercalations and move actin to the wound.

Why are syncytia better at closing wounds? To address this question, we considered the geometry of fusion. We observed that fusions sometimes occur between two adjacent cells equidistant from the wound, as diagramed in the top panel of Fig. 5A and exemplified in Fig. 1 I^{iii}-I^{iv} (cells 1,2) We call this type radial border breakdown, and it produces a syncytium elongated along the wound edge. Alternatively, fusion may occur between adjacent cells at different distances from the wound, as drawn in the lower panel of Fig. 5A and exemplified in

Fig. 1F (cells 3,4). We call this type tangential border breakdown, and it produces a spoke-like syncytium pointing into the wound. To analyze the frequency and timing of these two different axes of fusion, we calculated the angles of all lost borders for all border breakdowns in four wounds, binning them into radial and tangential fusions. (The angle of the axis of fusion can be determined for border breakdowns; the axis of fusion for shrinking cells is difficult to analyze, although the geometry of the starting cells must be similar.) In four wounds, 235 border breakdowns were identified: fewer radial borders broke down than tangential borders (39 vs 196), and radial borders broke down a bit later (Fig. 5B, Fig. S3B). However, the two types were similarly distributed around the wounds (Fig. S3A).

These fusion orientations provide different benefits for wound repair. Radial border fusions reduce the requirement for cell intercalation: as a wound closes, fewer cells can occupy the leading edge, necessitating a rearrangement of cell adhesions to allow cell intercalation, as depicted in the top of Fig. 5C. Indeed, intercalation is known to be a rate-limiting step of wound repair [23]. However, fusion of radial borders remove the need for intercalation, as shown in the bottom of Fig. 5C. To consider the contribution of radial border fusions to wound closure, we analyzed the three wounds from Fig. 4D-G and asked how many leading-edge cells fused radially vs. intercalated: 16-41% of cells removed from the leading edge were removed through fusion, reducing the burden of intercalation substantially (Fig. 5D). Interestingly, the larger the percentage of cells that fused rather than intercalated, the faster the wound closed (Fig. 5D). Thus, one mechanism syncytia use to promote wound closure is radial fusion.

In contrast, tangential border fusions might provide a way for cellular resources that would be trapped in distal cells to move toward the wound to contribute to closure. To test this hypothesis, we generated small flip-out clones expressing actin-GFP and wounded such that

unlabeled cells intervened between the labeled cell and the leading edge (Fig. 6). We envisioned that, upon fusion, actin would equilibrate throughout the newly fused cells, pooling their resources, and indeed we did observe actin-GFP to equilibrate between cells soon after fusing. For syncytia that did not have access to the leading edge (n =2), actin-GFP levels remained uniform (Fig. 6A,B). In contrast, syncytia with access to the leading edge (n = 10) first uniformly distributed actin (Fig. 6C^{ii}), but once the leading edge was contacted, they redistributed actin-GFP to it (Fig. 6C-D). Kymographs of actin-GFP confirm that regardless of location, actin equilibrates between fusing cells within 5 minutes (Fig. 6B^{iii}, D^{iv}); however, nearly all actin that originated in the distal cell is redistributed to the leading edge in a syncytium positioned there (Fig. 6D^{iv}). In one striking instance, actin-GFP appeared to travel through three cells to arrive at the leading edge from its initial location three rows back (Fig. 6E-G, Movie S4). Importantly, although actin is labeled from only one of the fusing cells, it likely represents the total actin from all fusing cells, explaining why syncytia are better able to occupy the leading edge. We envision that other resources would also be concentrated as needed by syncytia. We conclude that syncytia formed by cell fusion are able to outcompete their mononuclear neighbors by reducing intercalation and by concentrating the collected resources of many cells.

DISCUSSION:

Previous work established that polyploid cells – both cells with multiple nuclei and cells with single enlarged nuclei – are important for closing epithelial wounds in post-mitotic tissues [3]. Here we report that in a mitotic tissue, the epithelial monolayer of the pupal notum, syncytia form around wounds by cell fusion at a remarkably high rate, with almost half the epithelial cells within 5 cells of the wound fusing with neighbors over the course of hours. Syncytial size increases with wound size, indicating syncytia formation is a dynamic and scalable response to wounding. Syncytia form via two temporally distinct processes, a rapid breakdown of epithelial borders within 40 min of wounding, and later cell shrinking which persists 30 min to 2 h after wounding. We confirmed that both border breakdown and cell shrinking are cell fusion events, rather than epithelial to mesenchymal transitions or extrusions, by generating small clones of cells labeled with cytoplasmic GFP and observing the diffusion of GFP from a source cell into neighboring cells after wounding, indicating cell fusion. Strikingly, although the resulting syncytia are fewer in number than persisting diploid cells, they completely displace unfused cells at the leading edge of the wound such that wounds are closed entirely by syncytia.

We identified several factors that endow syncytia with wound closing abilities. Live imaging indicated that syncytia are faster than smaller cells at extending toward the wound, and once there, they maintain their positions at the leading edge, forcing out smaller cells. Epithelial wounds close by the cinching of an actin cable, sometimes called the purse string [24-27]; as the cable tightens and shortens, the leading edge becomes smaller, with room for fewer and fewer cells. Cells are removed from the leading edge by intercalation, a process that requires them to remodel their adhesions. A previous study found that intercalation is the rate-limiting step of wound closure; further, the greater the tension in cellular adhesions, the slower the wound

closure, a finding both predicted by computational modeling and verified experimentally. Thus, fluidity promotes closure [23]. By fusing, cells reduce the need for adhesion remodeling and intercalation as the leading edge becomes smaller. Moreover, the resulting larger cell has significantly more fluidity and less epithelial tension than the diploid progenitors, as recently demonstrated in syncytia formed by age-induced epidermal cell fusion [28].

In addition to promoting wound closure by reducing the burden of intercalation, syncytia can redirect toward the wound cellular resources that would be trapped in individual diploid cells. We demonstrated this ability by visualizing labeled actin from one cell as it fused with an unlabeled cell. As expected after fusion, labeled actin diffuses and equilibrates throughout the new large cell. Remarkably however, when the syncytium is in contact with the leading edge, labeled actin from the distal cell is concentrated at the leading edge, even if the original cell is several cells away from the leading edge. This result suggests that syncytia can apply up to N times more actin to the leading edge, where N represents the number of cells that fused; considering that we observed syncytia with dozens of nuclei, this could represent a significant enhancement of actin at the leading edge. Increased actin can explain the ability of syncytia to outcompete diploid cells at the leading edge. In addition to the actin purse-string, actin also forms filopodia and lamellipodia important for migration, offering an explanation for how syncytia extend more quickly than diploid neighbors toward the wound, and these structures also participate in closing the wound [27, 29]. Presumably, other resources such as mitochondria and ribosomes could also be pooled and concentrated by syncytia at cellular locations where they promote wound healing. It is known that mitochondrial fragmentation promotes the repair of single-cell wounds, with more fragmentation causing faster repair [30]. Further, fragmentation is localized to the site of cellular injury [31], raising the possibility that syncytia may increase the

local concentration of fragmented mitochondria. Ribosomes have been observed to be localized in wounded tissue, accumulating at the tips of severed neurons [32], and it is possible that syncytia may increase the localized pool of ribosomes in epidermal wounds. By pooling the cellular resources of component cells, syncytia may also allow lethally damaged cells to survive by providing them with needed survival factors originating in cells further from the wound. Thus, the concept of resource sharing that we demonstrate with actin may have ramifications for many resources.

We observed two cellular behaviors that attended fusion, border breakdowns and cell shrinking. Border breakdowns occurred sooner after wounding than shrinking and appeared to be a faster process, as shrinking lasted for hours. These differences in appearance and timing suggest that the mechanisms behind these fusions may be somewhat independent. For shrinking cells, we envision that the original site of cytoplasmic fusion, the fusion pore, occurs in the basolateral membrane, whereas border-breakdown fusion pores are nearer the apical adherens junctions observed to break down. The adherens junctions would be under more tension than the basolateral membranes, and this may explain why fusion proceeds more quickly there; we recently found that although epithelial tension drops after laser wounding, it is restored within about 10 min [33] , consistent with the timing of apical border breakdown.

It is unclear what triggers either type of wound-induced epithelial fusion. Many developmentally programmed cell fusions are mediated by fusogens, cell surface proteins that bring opposing membranes into close contact with each other, as in the *C. elegans* hypodermis [34-40]. For other cell fusions, the fusogen is elusive and may not exist, for example in *Drosophila* myoblast fusions, which occur when a fusion competent myoblast generates actin-rich podosome-like membrane protrusions that invade a founder cell [41-45], but we did not

observe these structures in fusing epidermal cells. Wound-induced fusion may be a response to the plasma membrane damage that occurs around wounds; indeed, plasma membrane damage has been documented around both laser wounds and puncture wounds [46-48].

Polyploidy as a wound response has begun to get increased recognition. In adult *Drosophila*, epithelial puncture wounds are repaired by both endoreplication and syncytia formation [3, 49-53]. In the zebrafish epicardium, genetic ablation is repaired by a wavefront of multinucleated polyploid cells formed by endomitosis, and these lead diploid cells to encompass the heart [1]. In adult mammalian cardiomyocytes, polyploidy may be an adaptive response to maintain growth after the cardiomyocytes lose their ability to complete mitosis. Mouse cornea endothelial cells endoreplicate to increase polyploidy to restore tissue ploidy following genetic ablation [52]. Mammalian hepatocytes are known to become increasingly polyploid with age [54, 55] and in response to various types of injury and disease [56-61]. All mechanisms that promote polyploidy – fusion, endomitosis, endoreplication – result in larger cells with the potential to localize more resources; of these, fusion would act the fastest after wounding because there is no need for DNA replication. Interestingly, in *Drosophila* embryos, wounds induce the surrounding cells to become larger by increasing their volume alone and not their ploidy [62], suggesting that simply an increase in size is important. Although many examples of wound-induced polyploidy exist, it is still likely to be an underreported phenomenon, as endpoint analysis might miss a transient polyploid response to injury; live imaging is the surest way to identify a polyploid wounding response.

Another polyploid response to injury can occur after surgical implantation of biomaterials for the purpose of guiding regeneration, as reviewed previously [8]. In some cases, only mononuclear cells of the immune system respond to the implant, and in these cases the

biomaterial is integrated into the body; in other cases, the implant triggers the fusion of immune cells into multinucleated giant cells, and in these cases the material is degraded and rejected. These multinucleated giant cells seem to share properties with the syncytia of the pupal notum, as they are formed by fusion in response to an environmental trigger and they have an aggressive ability to protect the animal in response to wounding. As these studies highlight, understanding the formation, maintenance, and regulation of polyploid cells may improve our ability to successfully implant biomaterials to aid tissue regeneration.

It is often noted that wound responses are similar to cancer cell behaviors. This similarity extends to wound-induced syncytia and their counterparts, polyploid giant cancer cells, as both cell types are highly aggressive and invasive. Chemotherapeutics induce the formation of polyploid giant cancer cells [63-66], and some studies indicate that they can form through cell-cell fusion in tumors [67-71]. Once formed polyploid giant cancer cells are hypothesized to escape further chemotherapy treatments due to increased resistance to genotoxic stress [72]. These polyploid giant cancer cells and their progeny also exhibit increased migration and invasion potential [73, 74]. The parallels between the behaviors of polyploid giant cancer cells and the wound-induced syncytia of the pupal notum highlight the importance of understanding wound induced syncytia formation in a highly reproducible system, as a basic understanding of how these cells form in the *Drosophila* notum could inform how they become dysregulated in cancer.

FIGURE LEGENDS:

Figure 1. Wounds induce epithelial syncytia via cell fusion.

A) Syncytia form within 2 h post wounding, evident by the clustering of multiple nuclei within cell borders. **B)** The number of nuclei per syncytia increases over time after wounding. Number of nuclei was estimated based on area and nuclear density (see text) for the 3 largest syncytia of 3 different wounds, mean and SD. **C-D)** Larger wounds generate larger syncytia. Images are at 3 h post wounding, single syncytium outlined. **E)** Apical area of three largest syncytia is proportional to initial wound size, mean and SD. **F)** A time course of six cells fusing within 30 min after wounding. Apical borders are lost (white arrowhead) as syncytia form. Original cells are numbered. **G)** All borders lost to cell fusion (white) mapped to cells in the first frame after wounding. The leading edge of wound closure will form at dashed line; cells within the shaded area were damaged by the wound and will be dismantled. **H)** Distance from the wound center vs time for all border breakdowns in 3 wounds. Each symbol represents a cell border. Leading-edge locations indicated by solid lines. **I)** Cytoplasmic GFP is expressed in cell 1 before wounding and mixes with neighboring cells 2-4 by 2 min after wounding. Cytoplasmic sharing is followed by the lagging fusion indicator of visible border breakdown (white arrow). The fates of cells 3 and 4 are shown at later times in Fig. 2D. Maximum intensity projections in A, C-D, G; single Z slices in F, I. Scales: A-D,G = 20 µm, F,I = 10 µm. W and red star indicate wound.

Figure 2: Cell fusion often appears as cell shrinking.

A) An epithelial cell (yellow arrow) shrinks in the epithelial plane after wounding. **(B)** Same sample as A, showing the shrinking cell's nucleus (asterisk) entering a neighboring syncytium, outlined in B^{iv}. **C)** Cell 1 expresses actin-GFP before wounding. After wounding, cell 1 fuses with cells 2-6 evidenced by GFP sharing, then cell 1 shrinks. **D)** Two cells shrink in the X-Y plane (white and yellow arrows in D^{i}-D^{iii}). X-Z projections are shown for each (D^{iv}-D^{vi} for the top yellow line; D^{vii}-D^{ix} for the lower white line). Rather than extrude, the shrinking cells'

cytoplasm moves to the right, to join with the neighboring wound-proximal syncytium, via basal connections. These frames are a continuation of the sample shown in Fig. 1I. **E)** All shrinking cells mapped to first frame after wounding. **F)** All shrinking cells and border breakdowns were tracked in 3 wounds. Border breakdown fusions happen sooner after wounding than shrinking fusions. A, B, C, D^{i-iii}, E show maximum intensity projections. D^{iv-ix} show X-Z projections. Scales: A, B, C, D^{i-iii}, E = 10 µm; D^{iv-ix} = 5 µm.

Figure 3: Half the cells near the wound fuse to form syncytia, demonstrated by tracking individual cell fates.

A) All GFP labeled cells in the region of fusion (80 µm) were tracked in 5 wounds over 6.5 h after wounding to determine frequency of fusion (GFP mixing) or persistence (no GFP mixing). Untrackable cells lost GFP, see Fig. S2A. **B)** Fusion is common within 70 µm. **C)** Shrinking-fusion and border-breakdown fusion occur at similar distances from the wound.

Figure 4: Syncytia outpace smaller cells.

A) Before wounding, two clusters of cells are labeled with GFP, 1-2 and 3-4 (white numbers). After wounding, cells 2 and 3 fuse with neighbors 5-9 to form a syncytium (dashed leading edge in Aiii), which advances toward the wound, passing unfused cell 4 (arrow). **B-C)** Unfused cell (outlined in orange and white) with corresponding nucleus (asterisk in C) is replaced at leading edge by neighboring syncytia (S and yellow outline, yellow arrows). **D)** All small cells are excluded from leading edge by syncytia well before the wound closes 20-160 min later. **E)** Images of sample 1 from the graph D. Unfused cells (arrows) were tracked over the course of wound closure and mapped back to the 30 min timepoint. **F)** At 120 min, the last unfused cell is

ejected from leading edge (arrow). The wound closed at 140 min. **G)** Percent of leading-edge perimeter occupied by syncytia increases to 100%. Images are single Z slices in A^{i}-A^{ii} and maximum intensity projections in A^{iii}-F. Scale: A,E-F = 20 µm, B-C = 10 µm.

Figure 5: Radial border fusions reduce the number of wound proximal intercalations. **A)** Illustration of tangential vs radial border breakdown. **B)** More tangential than radial borders break down after wounding. **C)** Radial border fusions reduce intercalation at a wound. **D)** Quantification of intercalations and fusions around the wounds of Fig. 4D,G.

Figure 6: Syncytia concentrate pooled resources at the leading edge.

Random scattered cells expressing Actin-GFP were generated by heat-shock mediated flip-out expression of Gal4. **A-B)** Labeled actin is expressed in cell 1 before wounding (A^{i}). Actin-GFP rapidly equilibrates between cells 1 and 2 by 28 minutes after wounding, demonstrating cytoplasmic fusion. At 180 min, cell 2 shrunk into cell 1. The resulting syncytiuym has no access to the leading edge, and actin remains equilibrated, as shown in the kymograph (B^{iii}) generated from actin-GFP intensity over time at the yellow line in B^{ii}. **C-D)** Labeled actin is expressed in cell 1 before wounding (C^{i}) and equilibrates between cells 1 and 2 by 6 minutes after wounding, demonstrating cytoplasmic fusion (C^{ii}). The resulting syncytium contacts the leading edge, and by 28 min after wounding actin from cell 1 is redistributed to the wound margin by 28 min after wounding, as shown in the kymograph (D^{iv}) of actin intensity over time at the yellow line in D^{iii}. At 55 min after wounding, cell 1 shrunk into cell 2. **E-F)** Before wounding, actin-GFP in cell 1 is three cells away from the future leading edge. After wounding, fusion of cells 1-4 allows actin-GFP to move to and accumulate at the leading-edge actin cable. Border breakdown occurs between cells 1-2 (E^{v}) which later shrink into cells 3,4 (see Movie S4). **G)** Mean profile plot of

actin-GFP comparing the syncytia in F^{v} at 30 min after wounding (dark line) with the cells in F^{i} before wounding (dotted line) demonstrating that nearly all actin-GFP has been redistributed to the leading edge from its starting position 20-30 µm away. Single Z slices for $E^{i - ii}$, $F^{i - ii}$; maximum intensity projections for A-D, $E^{iii - v}$, $F^{iii - v}$. Scale A-B^{ii}, C^{i}-D^{iii} = 5 µm, E-F = 10 µm.

Supplemental Movie 1: Syncytial cells form after wounding in the *Drosophila* pupal notum. Epithelial cell borders in red (p120ctnRFP) and nuclei in green (HistoneGFP). White box on first frame denotes field of view in Fig. 1A. Movie begins before wounding and extends to 2 h after wounding.

Supplemental Movie 2: GFP mixing precedes border breakdown after wounding. Arrow in first frame points to cell border between cells that will fuse after wounding. GFP diffusion into the unlabeled cell precedes visible border breakdown. w, wound region. Cell borders are labeled with p120ctnRFP. Movie begins before wounding and extends to 2 h 10 min after wounding. Same cells as Fig. 1I and 2D.

Supplemental Movie 3: Shrinking cells contribute to syncytia. Arrow in first frame points to an individual cell labeled with Actin-GFP that fuses by shrinking after wounding. This cell contributes its actin-GFP to neighboring cells minutes after wounding then shrinks much later; shrinking is first evident about 1.5 h after wounding and is nearly complete by 3.5 h after wounding. w, wound region. Cell borders are labeled with p120ctnRFP. Same cells as Fig. 2C.

Supplemental Movie 4: Syncytia pool actin and concentrate it at the leading edge of repair. An individual cell labeled with actin-GFP fuses with wound proximal cells and contributes its actin to the leading edge of the syncytium. w, wound region. The original source cell and its immediate neighbor go on to shrink into wound proximal cells. Cell borders are labeled with p120ctnRFP. Same cells as Fig. 6E,F.

Acknowledgements: We thank James O'Connor for his original observations of syncytial cells around pupal wounds, and Kimi LaFever Hodge for technical assistance. We thank the BDRC for fly stocks. J.S.W. was supported by T32HD007502. This work was supported by the National Institute of General Medical Sciences R01GM130130 to APM and MSH.

METHODS

Key Resources Table				
Reagent type (species) or resource	**Designation**	**Source or reference**	**Identifiers**	**Additional information**
Fly line (*Drosophila melanogaster*)	"HistoneGFP"	BDSC:	24163	w[*]; P{w[+mC]=His2Av-EGFP.C}2/SM6a
Fly line (*Drosophila melanogaster*)	"p120ctnRFP"	(obtained as a gift from Shigeo Hayashi[21])		y; ubiP-p120ctn-TagRFP
Fly line (*Drosophila melanogaster*)	"AyGal4"	BDSC:	3953	w[1118]; P{w[+mC]=AyGAL4}25/CyO
Fly line (*Drosophila melanogaster*)	"hsFLP"	BDSC:	55813	w[1118]; P{y[+t7.7] w[+mC]=hs-FLPD5}attP2
Fly line (*Drosophila melanogaster*)	"GFP"	BDSC:	1521	w[*]; P{w[+mC]=UAS-GFP.S65T}eg[T10]
Fly line (*Drosophila melanogaster*)	"Actin-GFP"	BDSC:	7310	w[1118]; P{w[+mC]=UASp-Act5C.T:GFP}2; l(3)*[*]/TM6C, Sb[1] Tb[1]
Fly line (*Drosophila melanogaster*)	"MyosinII-GFP"	BDSC:	51564	w[*]; P{w[+mC]=PTT-GC}zip[CC01626]/SM6a
Fly line (*Drosophila melanogaster*)	“HistoneRFP”	BDSC:	23651	yw; His2AvRFP / (CyO)
Software	FIJI	Schindelin et al., 2012	RRID: SCR_002285	

Software	NIS Elements	Nikon Instruments Inc.	RRID: SCR_002285	
Software	Microsoft Excel	Microsoft	https://www.microsoft.com/en-us/microsoft-365/excel	
Software	GraphPad Prism 9	GraphPad	https://www.graphpad.com/scientific-software/prism/	
Software	Affinity Designer	Affinity Serif	https://affinity.serif.com/en-us/designer/	

Resource availability

Lead contact

Requests for fly lines, reagents, and additional questions should be directed to Dr. Andrea Page-McCaw (andrea.page-mccaw@vanderbilt.edu)

Materials availability

Fly lines generated in this study are available from the Bloomington *Drosophila* Stock Center or from the lead contact.

Data availability

All microscopy movies have been stored on Dropbox and can be made available for download upon request.

Experimental model and subject details

Drosophila melanogaster

Drosophila lines used in this study are in Table S1. All *Drosophila* lines were maintained on standard cornmeal-molasses media supplemented with dry yeast. All flies, except those used in

heat-shock flip clonal analysis, were raised at room temperature. For clonal analysis experiments flies were raised at 18 degrees Celsius until the 3rd instar stage when they were heat shocked in a circulating water bath at 37 degrees Celsius for 3 minutes. They were then allowed to develop at room temperature to 15-18hr after puparium formation (APF) before wounding experiments (described below) were conducted.

Method details

Pupal mounting

At room temperature, white prepupae were identified and marked within plastic food vials. Pupae were allowed to age until the 15-18 APF stage. 15-18 APF pupae were then removed from the vial onto a piece of double-sided tape (Scotch brand, catalogue #665) applied to a microscope slide. Using fine forceps, the anterior pupal case was removed exposing the head and notum of all pupae applied to the tape, as previously described in [46, 75]. The tape was carefully removed from the microscope slide and inverted onto a pre-prepared cover glass (Corning 2980-246, 24 mm x 64 mm) [76]. The pupae were carefully pressed down onto the cover glass by adhering the section of tape above the pupal head. Once the notum was visibly pressed onto the cover glass an oxygen permeable membrane (YSI, standard membrane kit, cat#1329882) was applied to prevent the pupae from drying out during imaging.

Pupal survival

Following imaging, pupae were kept mounted as described above and allowed to continue to develop and eclose for 3-4 days. Pupae that continued developing until they were able to crawl out of the partially dissected case were classified as ‘survived’ and their data acquired form these samples were used for analysis. If a pupae did not survive to eclosion, the associated datasets were not used in the study.

Live imaging

Images were collected using a Nikon Ti2 Eclipse with X-light V2 spinning disc (Nikon, Tokyo, Japan) with a 40X 1.3 NA oil-immersion objective or 60X 1.4 NA oil-immersion objective. Unless otherwise noted samples were imaged pre-wounding, immediately after wounding, every 2 min for 30 min, and then every 10 min for 6 h. Images were pre-processed in NIS-Elements using combinations of background subtraction, rolling ball correction, local contrast, and Denoise a.i. Assembly of figure panels was done using Affinity Designer and frames were centered on the entity in focus, compensating for frame shift due to wounding.

Laser ablation

A single pulse of a 3rd harmonic (355 nm) Q-switched Nd:YAG laser (5 ns pulse-width, Continuum Minilite II, Santa Clara, CA) was used for laser ablation. Laser pulse energies were kept to 1.9 μJ +/- 0.1 μJ, increased from our previously report [77] to keep the wound size similar between old and new ablation rig.

Border breakdown and tangential vs radial assignment analysis

Individual border breakdown events were manually observed using FIJI by identifying syncytia late in the movie and back-tracking to determine which borders broke down to form them. Each border that was broken down was traced back to the first frame after wounding to develop the map on Fig 1G. For each border breakdown, distance from the center of the wound and time after wounding were recorded in Microsoft excel. Border breakdown events were categorized as tangential or radial based on the orientation of the border relative to a vector pointing outward from the center of the wound. Specifically, the line tool in FIJI was used to measure both the angle of the border with respect to the horizon, theta, and the angle of the line from the center of the wound to the center of the border with respect to the horizon, alpha. If cos(alpha-theta) was

less than cos(45 degrees), then the border was classified as tangential. Otherwise, the border was classified as radial.

Shrinking cell initiation / duration analysis

Shrinking cells were identified in live microscopy movies by beginning at the end of the movie and playing backwards in FIJI. Backwards, a shrinking cell appears to bloom from the epithelial layer, characterized by the expansion of a bright puncta of p120ctnRFP. Each cell that underwent this behavior was marked on a single frame of the movie, then the distance from the center of the wound when shrinking started was denoted as well as the time that the shrinking started and completed. All cells that shrank were then manually traced back to the first frame after wounding to develop the map of shrinking cells (Fig 2E).

Approximating nuclei per syncytia

Nuclei and cell borders do not align in Z-projections of the pupal notum as the cells are non-prismatic. To estimate the number of nuclei per syncytium, the pre-wounding density of nuclei per unit area was determined for the circular region where syncytia form after wounding. Next, the apical area of the three largest syncytia/cells around a wound was measured at 0h, 1 h and 2 h post wounding. The area of each syncytia was multiplied by the nuclear density to yield the approximate number of nuclei per syncytia. The number of nuclei in each of the three syncytia was averaged to give a value for each of three samples in Fig. 1B.

Measuring apical area of syncytia across varied wound sizes

The three largest syncytia were determined by eye in FIJI for six samples, three ablated at 1.9 µJ and three ablated at 3 µJ ablation. The apical area of syncytia was measured 3 h post wounding using the p120ctnRFP signal. Initial wound size was calculated by measuring Myosin II marked leading edge when it became apparent 30-160 min post wounding.

Unfused cells at leading edge: count and percent analysis

Unfused cells at the leading edge were identified using FIJI by a lack of border breakdowns. Each unfused cell was manually observed over the duration of wound closure and the time at which it departed from the leading edge was noted. A count of unfused cells at the leading edge was created in Excel and formal graphs were generated using Prism 9. To measure percent of the leading edge comprised of unfused vs. syncytial cells, each unfused cell's leading edge contact was measured in FIJI using the polygon line tool. The total circumference of the wound was measured using the polygon line tool and unfused cell measurements were subtracted from the total to infer the syncytial occupancy at the leading edge. Formal histograms were generated using Prism 9.

Analyzing GFP labeled cells

107 individually labeled GFP cells were analyzed across 5 wounds over 6.5 h. The position of the ablation was optimized to place as many individually labeled cells within 40-80um from the center of the wound as possible. After wounding it was possible to identify a mixing event by the decrease in intensity from the source cell with a corresponding increase in intensity of a previously unlabeled neighbor. Intensity differences made it possible to distinguish instances where two source cells were adjacent to each other but only one had a mixing event. However, large patches of source cells were not evaluated because inter-patch mixing was not distinguishable. To evaluate if border breakdowns were preceded by mixing, the 11 individually labeled cells that had border breakdowns were tracked back to the start of the movie and confirmed to have a mixing event. There was never an instance where a labeled source cell had a border breakdown without a prior mixing event occurring.

Wound Closure Analysis

A pigmented scar forms at the site of laser ablation making identifying the exact moment a wound is closed difficult. Since the scar is approximately the same size in each sample, the time point at which the Myosin II signal disappeared below the scar was used as a proxy for closure.

Calculating Intercalation

The change in the number of cells when the leading edge forms at 30 min (N_{start}) to when the wound is closed (N_{end}) is equal to the number of intercalations plus the number of radial fusion events. Thus, (intercalations = ΔN – radial fusions). For the same three samples used in Fig 4D,G, we determined ΔN from N_{start} at 30 min and N_{end} when the wound had closed. Radial fusions were tallied by manually observing border breakdown events between the leading-edge cells and intercalations were calculated. Each radial fusion was counted as one prevented intercalation event.

Kymograph and plot profile analysis

Actin-GFP intensity was analyzed using the kymograph tool in FIJI after drawing a 11-pixel line through the middle of the syncytia. Profile plot values were exported from NIS elements to Excel and graphs were generated using Prism.

REFERENCES

1. Cao, J., Wang, J., Jackman, C.P., Cox, A.H., Trembley, M.A., Balowski, J.J., Cox, B.D., De Simone, A., Dickson, A.L., Di Talia, S., et al. (2017). Tension Creates an Endoreplication Wavefront that Leads Regeneration of Epicardial Tissue. Dev Cell *42*, 600-615.e604.
2. Park, S., Gonzalez, D.G., Guirao, B., Boucher, J.D., Cockburn, K., Marsh, E.D., Mesa, K.R., Brown, S., Rompolas, P., Haberman, A.M., et al. (2017). Tissue-scale coordination of cellular behaviour promotes epidermal wound repair in live mice. Nat Cell Biol *19*, 155-163.
3. Losick, V.P., Fox, D.T., and Spradling, A.C. (2013). Polyploidization and cell fusion contribute to wound healing in the adult Drosophila epithelium. Curr Biol *23*, 2224-2232.
4. Tamori, Y., and Deng, W.M. (2013). Tissue repair through cell competition and compensatory cellular hypertrophy in postmitotic epithelia. Dev Cell *25*, 350-363.
5. Nandakumar, S., Grushko, O., and Buttitta, L.A. (2020). Polyploidy in the adult Drosophila brain. Elife *9*.
6. Galko, M.J., and Krasnow, M.A. (2004). Cellular and Genetic Analysis of Wound Healing in Drosophila Larvae. PLoS Biol *2*, e239.
7. Wang, Y., Antunes, M., Anderson, A.E., Kadrmas, J.L., Jacinto, A., and Galko, M.J. (2015). Integrin Adhesions Suppress Syncytium Formation in the Drosophila Larval Epidermis. Curr Biol *25*, 2215-2227.
8. Al-Maawi, S., Orlowska, A., Sader, R., James Kirkpatrick, C., and Ghanaati, S. (2017). In vivo cellular reactions to different biomaterials-Physiological and pathological aspects and their consequences. Semin Immunol *29*, 49-61.
9. Davies, P.S., Powell, A.E., Swain, J.R., and Wong, M.H. (2009). Inflammation and Proliferation Act Together to Mediate Intestinal Cell Fusion. PloS one *4*, e6530.
10. Alvarez-Dolado, M., Pardal, R., Garcia-Verdugo, J.M., Fike, J.R., Lee, H.O., Pfeffer, K., Lois, C., Morrison, S.J., and Alvarez-Buylla, A. (2003). Fusion of bone-marrow-derived cells with Purkinje neurons, cardiomyocytes and hepatocytes. Nature *425*, 968-973.
11. Corbel, S.Y., Lee, A., Yi, L., Duenas, J., Brazelton, T.R., Blau, H.M., and Rossi, F.M. (2003). Contribution of hematopoietic stem cells to skeletal muscle. Nat Med *9*, 1528-1532.
12. Nygren, J.M., Jovinge, S., Breitbach, M., Säwén, P., Röll, W., Hescheler, J., Taneera, J., Fleischmann, B.K., and Jacobsen, S.E. (2004). Bone marrow-derived hematopoietic cells generate cardiomyocytes at a low frequency through cell fusion, but not transdifferentiation. Nat Med *10*, 494-501.
13. Kim, J.H., Jin, P., Duan, R., and Chen, E.H. (2015). Mechanisms of myoblast fusion during muscle development. Current opinion in genetics & development *32*, 162-170.
14. Lehka, L., and Rędowicz, M.J. (2020). Mechanisms regulating myoblast fusion: A multilevel interplay. Seminars in Cell & Developmental Biology *104*, 81-92.
15. Podbilewicz, B., and White, J.G. (1994). Cell fusions in the developing epithelial of C. elegans. Dev Biol *161*, 408-424.
16. Renaud, S.J., and Jeyarajah, M.J. (2022). How trophoblasts fuse: an in-depth look into placental syncytiotrophoblast formation. Cellular and Molecular Life Sciences *79*, 433.
17. Søe, K. (2020). Osteoclast Fusion: Physiological Regulation of Multinucleation through Heterogeneity-Potential Implications for Drug Sensitivity. Int J Mol Sci *21*.
18. Leroy, H., Han, M., Woottum, M., Bracq, L., Bouchet, J., Xie, M., and Benichou, S. (2020). Virus-Mediated Cell-Cell Fusion. Int J Mol Sci *21*.
19. Pawelek, J.M., and Chakraborty, A.K. (2008). Fusion of tumour cells with bone marrow-derived cells: a unifying explanation for metastasis. Nature Reviews Cancer *8*, 377-386.

20. Guirao, B., Rigaud, S.U., Bosveld, F., Bailles, A., López-Gay, J., Ishihara, S., Sugimura, K., Graner, F., and Bellaïche, Y. (2015). Unified quantitative characterization of epithelial tissue development. eLife *4*, e08519.
21. Ogura, Y., Wen, F.-L., Sami, M.M., Shibata, T., and Hayashi, S. (2018). A Switch-like Activation Relay of EGFR-ERK Signaling Regulates a Wave of Cellular Contractility for Epithelial Invagination. Developmental Cell *46*, 162-172.e165.
22. Pignoni, F., and Zipursky, S.L. (1997). Induction of Drosophila eye development by Decapentaplegic. Development *124*, 271-278.
23. Tetley, R.J., Staddon, M.F., Heller, D., Hoppe, A., Banerjee, S., and Mao, Y. (2019). Tissue Fluidity Promotes Epithelial Wound Healing. Nat Phys *15*, 1195-1203.
24. Bement, W.M., Forscher, P., and Mooseker, M.S. (1993). A novel cytoskeletal structure involved in purse string wound closure and cell polarity maintenance. J. Cell Biol. *121*, 565-578.
25. Tamada, M., Perez, T.D., Nelson, W.J., and Sheetz, M.P. (2007). Two distinct modes of myosin assembly and dynamics during epithelial wound closure. J. Cell Biol. *176*, 27-33.
26. Martin, P., and Lewis, J. (1992). Actin cables and epidermal movement in embryonic wound healing. Nature *360*, 179-183.
27. Abreu-Blanco, M.T., Verboon, J.M., Liu, R., Watts, J.J., and Parkhurst, S.M. (2012). Drosophila embryos close epithelial wounds using a combination of cellular protrusions and an actomyosin purse string. J Cell Sci *125*, 5984-5997.
28. Dehn, A.S., Duhaime, L., Gogna, N., Nishina, P.M., Kelly, K., and Losick, V.P. (2023). Epithelial mechanics are maintained by inhibiting cell fusion with age in Drosophila. Journal of Cell Science.
29. Farooqui, R., and Fenteany, G. (2005). Multiple rows of cells behind an epithelial wound edge extend cryptic lamellipodia to collectively drive cell-sheet movement. Journal of Cell Science *118*, 51-63.
30. Fu, H., Zhou, H., Yu, X., Xu, J., Zhou, J., Meng, X., Zhao, J., Zhou, Y., Chisholm, A.D., and Xu, S. (2020). Wounding triggers MIRO-1 dependent mitochondrial fragmentation that accelerates epidermal wound closure through oxidative signaling. Nature communications *11*, 1050.
31. Horn, A., Raavicharla, S., Shah, S., Cox, D., and Jaiswal, J.K. (2020). Mitochondrial fragmentation enables localized signaling required for cell repair. J Cell Biol *219*.
32. Noma, K., Goncharov, A., Ellisman, M.H., and Jin, Y. (2017). Microtubule-dependent ribosome localization in C. elegans neurons. eLife *6*, e26376.
33. Han, I., Nassar, L.S., Page-McCaw, A., and Hutson, M.S. (2023). After wounding, a G-protein coupled receptor restores tension to epithelial cells in a dynamic inward-traveling wave. bioRxiv.
34. Chernomordik, L.V., and Kozlov, M.M. (2008). Mechanics of membrane fusion. Nature Structural & Molecular Biology *15*, 675-683.
35. Markvoort, A.J., and Marrink, S.J. (2011). Chapter 11 - Lipid Acrobatics in the Membrane Fusion Arena. In Current Topics in Membranes, Volume 68, L.V. Chernomordik and M.M. Kozlov, eds. (Academic Press), pp. 259-294.
36. Mohler, W.A., Shemer, G., del Campo, J.J., Valansi, C., Opoku-Serebuoh, E., Scranton, V., Assaf, N., White, J.G., and Podbilewicz, B. (2002). The type I membrane protein EFF-1 is essential for developmental cell fusion. Developmental cell *2*, 355-362.
37. Podbilewicz, B., Leikina, E., Sapir, A., Valansi, C., Suissa, M., Shemer, G., and Chernomordik, L.V. (2006). The C. elegans developmental fusogen EFF-1 mediates homotypic fusion in heterologous cells and in vivo. Developmental cell *11*, 471-481.
38. Shemer, G., Suissa, M., Kolotuev, I., Nguyen, K.C., Hall, D.H., and Podbilewicz, B. (2004). EFF-1 is sufficient to initiate and execute tissue-specific cell fusion in C. elegans. Current Biology *14*, 1587-1591.

641 39. Sapir, A., Choi, J., Leikina, E., Avinoam, O., Valansi, C., Chernomordik, L.V., Newman, A.P., and
642 Podbilewicz, B. (2007). AFF-1, a FOS-1-regulated fusogen, mediates fusion of the anchor cell in C.
643 elegans. Developmental cell *12*, 683-698.
644 40. Iosilevskii, Y., and Podbilewicz, B. (2021). Chapter Seven - Programmed cell fusion in
645 development and homeostasis. In Current Topics in Developmental Biology, Volume 144, S.
646 Jarriault and B. Podbilewicz, eds. (Academic Press), pp. 215-244.
647 41. Rushton, E., Drysdale, R., Abmayr, S.M., Michelson, A.M., and Bate, M. (1995). Mutations in a
648 novel gene, myoblast city, provide evidence in support of the founder cell hypothesis for
649 Drosophila muscle development. Development *121*, 1979-1988.
650 42. Sens, K.L., Zhang, S., Jin, P., Duan, R., Zhang, G., Luo, F., Parachini, L., and Chen, E.H. (2010). An
651 invasive podosome-like structure promotes fusion pore formation during myoblast fusion. J Cell
652 Biol *191*, 1013-1027.
653 43. Kim, J.H., Ren, Y., Ng, W.P., Li, S., Son, S., Kee, Y.S., Zhang, S., Zhang, G., Fletcher, D.A., Robinson,
654 D.N., et al. (2015). Mechanical tension drives cell membrane fusion. Dev Cell *32*, 561-573.
655 44. Lee, D.M., and Chen, E.H. (2019). Drosophila Myoblast Fusion: Invasion and Resistance for the
656 Ultimate Union. Annu Rev Genet *53*, 67-91.
657 45. Petrany, M.J., and Millay, D.P. (2019). Cell Fusion: Merging Membranes and Making Muscle.
658 Trends Cell Biol *29*, 964-973.
659 46. Shannon, E.K., Stevens, A., Edrington, W., Zhao, Y., Jayasinghe, A.K., Page-McCaw, A., and
660 Hutson, M.S. (2017). Multiple Mechanisms Drive Calcium Signal Dynamics around Laser-Induced
661 Epithelial Wounds. Biophys J *113*, 1623-1635.
662 47. O'Connor, J., Akbar, F.B., Hutson, M.S., and Page-McCaw, A. (2021). Zones of cellular damage
663 around pulsed-laser wounds. PloS one *16*, e0253032.
664 48. McNeil, P.L., and Steinhardt, R.A. (2003). Plasma membrane disruption: repair, prevention,
665 adaptation. Annu Rev Cell Dev Biol *19*, 697-731.
666 49. Besen-McNally, R., Gjelsvik, K.J., and Losick, V.P. (2021). Wound-induced polyploidization is
667 dependent on Integrin-Yki signaling. Biology Open *10*, bio055996.
668 50. Au - Bailey, E.C., Au - Dehn, A.S., Au - Gjelsvik, K.J., Au - Besen-McNally, R., and Au - Losick, V.P.
669 (2020). A Drosophila Model to Study Wound-induced Polyploidization. JoVE, e61252.
670 51. Grendler, J., Lowgren, S., Mills, M., and Losick, V.P. (2019). Wound-induced polyploidization is
671 driven by Myc and supports tissue repair in the presence of DNA damage. Development *146*.
672 52. Losick, V.P., Jun, A.S., and Spradling, A.C. (2016). Wound-Induced Polyploidization: Regulation by
673 Hippo and JNK Signaling and Conservation in Mammals. PloS one *11*, e0151251.
674 53. Losick, V.P. (2016). Wound-Induced Polyploidy Is Required for Tissue Repair. Adv Wound Care
675 (New Rochelle) *5*, 271-278.
676 54. Carriere, R. (1969). The growth of liver parenchymal nuclei and its endocrine regulation.
677 International review of cytology *25*, 201-277.
678 55. Wheatley, D. (2008). Growing evidence of the repopulation of regressed tumours by the division
679 of giant cells. Cell Biology International *32*, 1029-1030.
680 56. Toyoda, H., Bregerie, O., Vallet, A., Nalpas, B., Pivert, G., Brechot, C., and Desdouets, C. (2005).
681 Changes to hepatocyte ploidy and binuclearity profiles during human chronic viral hepatitis. Gut
682 *54*, 297-302.
683 57. Gentric, G., Maillet, V., Paradis, V., Couton, D., L'Hermitte, A., Panasyuk, G., Fromenty, B.,
684 Celton-Morizur, S., and Desdouets, C. (2015). Oxidative stress promotes pathologic
685 polyploidization in nonalcoholic fatty liver disease. J Clin Invest *125*, 981-992.
686 58. Madra, S., Styles, J., and Smith, A.G. (1995). Perturbation of hepatocyte nuclear populations
687 induced by iron and polychlorinated biphenyls in C57BL/10ScSn mice during carcinogenesis.
688 Carcinogenesis *16*, 719-727.

59. Muramatsu, Y., Yamada, T., Moralejo, D.H., Mochizuki, H., Sogawa, K., and Matsumoto, K. (2000). Increased polyploid incidence is associated with abnormal copper accumulation in the liver of LEC mutant rat. Research Communications in Molecular Pathology and Pharmacology *107*, 129-136.
60. Wilkinson, P.D., Alencastro, F., Delgado, E.R., Leek, M.P., Weirich, M.P., Otero, P.A., Roy, N., Brown, W.K., Oertel, M., and Duncan, A.W. (2019). Polyploid Hepatocytes Facilitate Adaptation and Regeneration to Chronic Liver Injury. Am J Pathol *189*, 1241-1255.
61. Sigal, S.H., Rajvanshi, P., Gorla, G.R., Sokhi, R.P., Saxena, R., Gebhard Jr, D.R., Reid, L.M., and Gupta, S. (1999). Partial hepatectomy-induced polyploidy attenuates hepatocyte replication and activates cell aging events. American Journal of Physiology-Gastrointestinal and Liver Physiology *276*, G1260-G1272.
62. Scepanovic, G., Hunter, M.V., Kafri, R., and Fernandez-Gonzalez, R. (2021). p38-mediated cell growth and survival drive rapid embryonic wound repair. Cell Reports *37*, 109874.
63. Wang, Y., Wang, Y., and Zheng, W. (2013). Cytologic changes of ovarian epithelial cancer induced by neoadjuvant chemotherapy. Int J Clin Exp Pathol *6*, 2121-2128.
64. Illidge, T.M., Cragg, M.S., Fringes, B., Olive, P., and Erenpreisa, J.A. (2000). Polyploid giant cells provide a survival mechanism for p53 mutant cells after DNA damage. Cell Biol Int *24*, 621-633.
65. Ogden, A., Rida, P.C.G., Knudsen, B.S., Kucuk, O., and Aneja, R. (2015). Docetaxel-induced polyploidization may underlie chemoresistance and disease relapse. Cancer Letters *367*, 89-92.
66. Mosieniak, G., Sliwinska, M.A., Alster, O., Strzeszewska, A., Sunderland, P., Piechota, M., Was, H., and Sikora, E. (2015). Polyploidy Formation in Doxorubicin-Treated Cancer Cells Can Favor Escape from Senescence. Neoplasia *17*, 882-893.
67. Melzer, C., von der Ohe, J., and Hass, R. (2018). In Vitro Fusion of Normal and Neoplastic Breast Epithelial Cells with Human Mesenchymal Stroma/Stem Cells Partially Involves Tumor Necrosis Factor Receptor Signaling. Stem Cells *36*, 977-989.
68. Noubissi, F.K., Harkness, T., Alexander, C.M., and Ogle, B.M. (2015). Apoptosis-induced cancer cell fusion: a mechanism of breast cancer metastasis. The FASEB Journal *29*, 4036-4045.
69. Zhang, H., Ma, H., Yang, X., Fan, L., Tian, S., Niu, R., Yan, M., Zheng, M., and Zhang, S. (2021). Cell Fusion-Related Proteins and Signaling Pathways, and Their Roles in the Development and Progression of Cancer. Front Cell Dev Biol *9*, 809668.
70. Song, Y., Zhao, Y., Deng, Z., Zhao, R., and Huang, Q. (2021). Stress-Induced Polyploid Giant Cancer Cells: Unique Way of Formation and Non-Negligible Characteristics. Front Oncol *11*, 724781.
71. Powell, A.E., Anderson, E.C., Davies, P.S., Silk, A.D., Pelz, C., Impey, S., and Wong, M.H. (2011). Fusion between Intestinal epithelial cells and macrophages in a cancer context results in nuclear reprogramming. Cancer Res *71*, 1497-1505.
72. Weihua, Z., Lin, Q., Ramoth, A.J., Fan, D., and Fidler, I.J. (2011). Formation of solid tumors by a single multinucleated cancer cell. Cancer *117*, 4092-4099.
73. Zhao, Q., Zhang, K., Li, Z., Zhang, H., Fu, F., Fu, J., Zheng, M., and Zhang, S. (2021). High Migration and Invasion Ability of PGCCs and Their Daughter Cells Associated With the Nuclear Localization of S100A10 Modified by SUMOylation. Front Cell Dev Biol *9*, 696871.
74. Qu, Y., Zhang, L., Rong, Z., He, T., and Zhang, S. (2013). Number of glioma polyploid giant cancer cells (PGCCs) associated with vasculogenic mimicry formation and tumor grade in human glioma. J Exp Clin Cancer Res *32*, 75.
75. James T. O'Connor, E.K.S., M. Shane Hutson, Andrea Page-McCaw (In revision at STAR Protocols). Mounting Drosophila pupae for laser ablation and live imaging of the dorsal thorax. STAR Protocols.

76. O'Connor, J.T., Shannon, E.K., Hutson, M.S., and Page-McCaw, A. (2022). Mounting Drosophila pupae for laser ablation and live imaging of the dorsal thorax. STAR Protoc *3*, 101396.
77. O'Connor, J.T., Stevens, A.C., Shannon, E.K., Akbar, F.B., LaFever, K.S., Narayanan, N.P., Gailey, C.D., Hutson, M.S., and Page-McCaw, A. (2021). Proteolytic activation of Growth-blocking peptides triggers calcium responses through the GPCR Mthl10 during epithelial wound detection. Dev Cell *56*, 2160-2175.e2165.

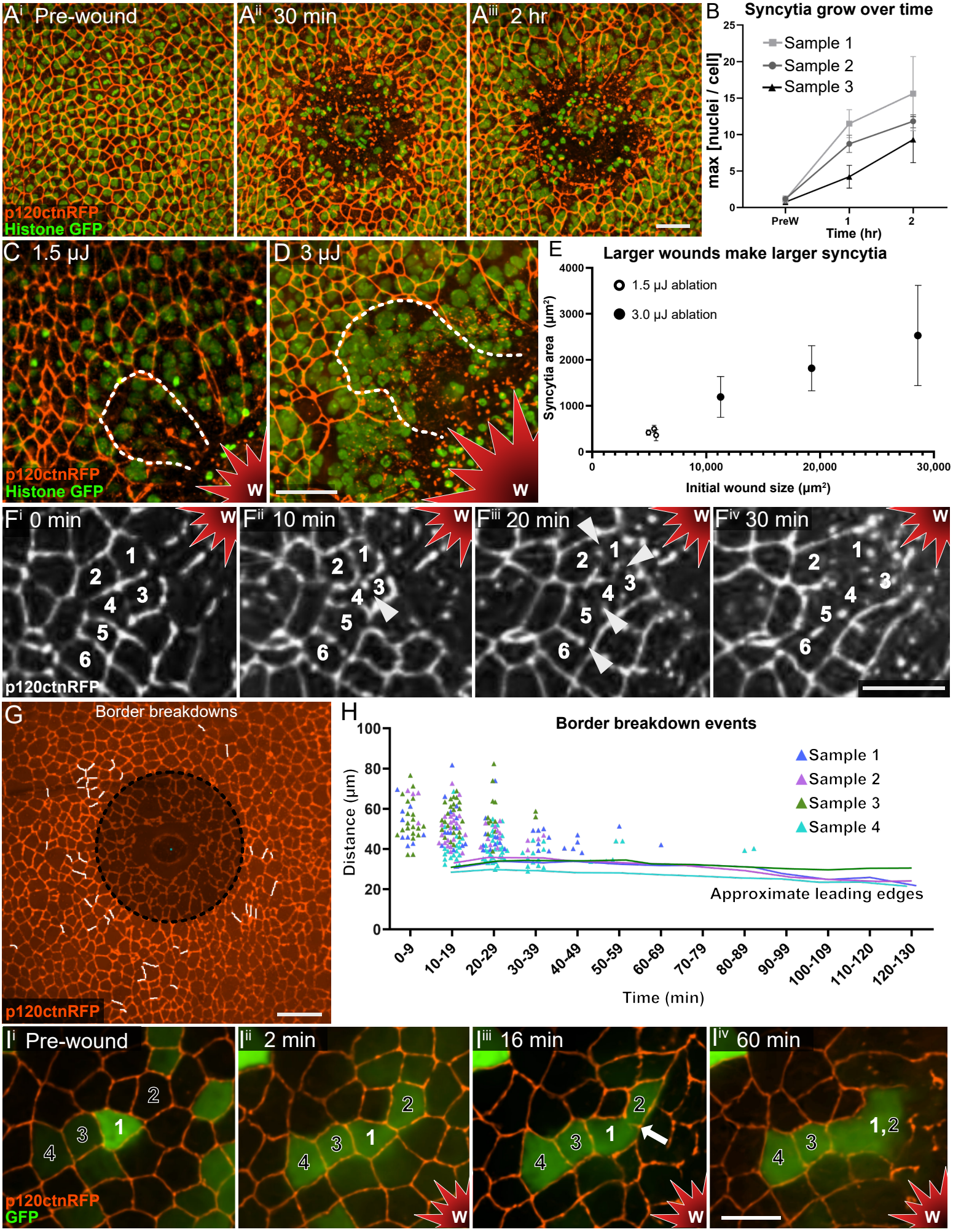
Ai Pre-wound
Aii 30 min
Aiii 2 hr
p120ctnRFP
Histone GFP
B
Syncytia grow over time
Sample 1
Sample 2
Sample 3
max [nuclei / cell]
Time (hr)
PreW
C 1.5 μJ
D 3 μJ
W
E
Larger wounds make larger syncytia
1.5 μJ ablation
3.0 μJ ablation
Syncytia area (μm²)
Initial wound size (μm²)
Fi 0 min
Fii 10 min
Fiii 20 min
Fiv 30 min
G
Border breakdowns
H
Border breakdown events
Sample 1
Sample 2
Sample 3
Sample 4
Distance (μm)
Approximate leading edges
Time (min)
Ii Pre-wound
Iii 2 min
Iii 16 min
Iiv 60 min
GFP

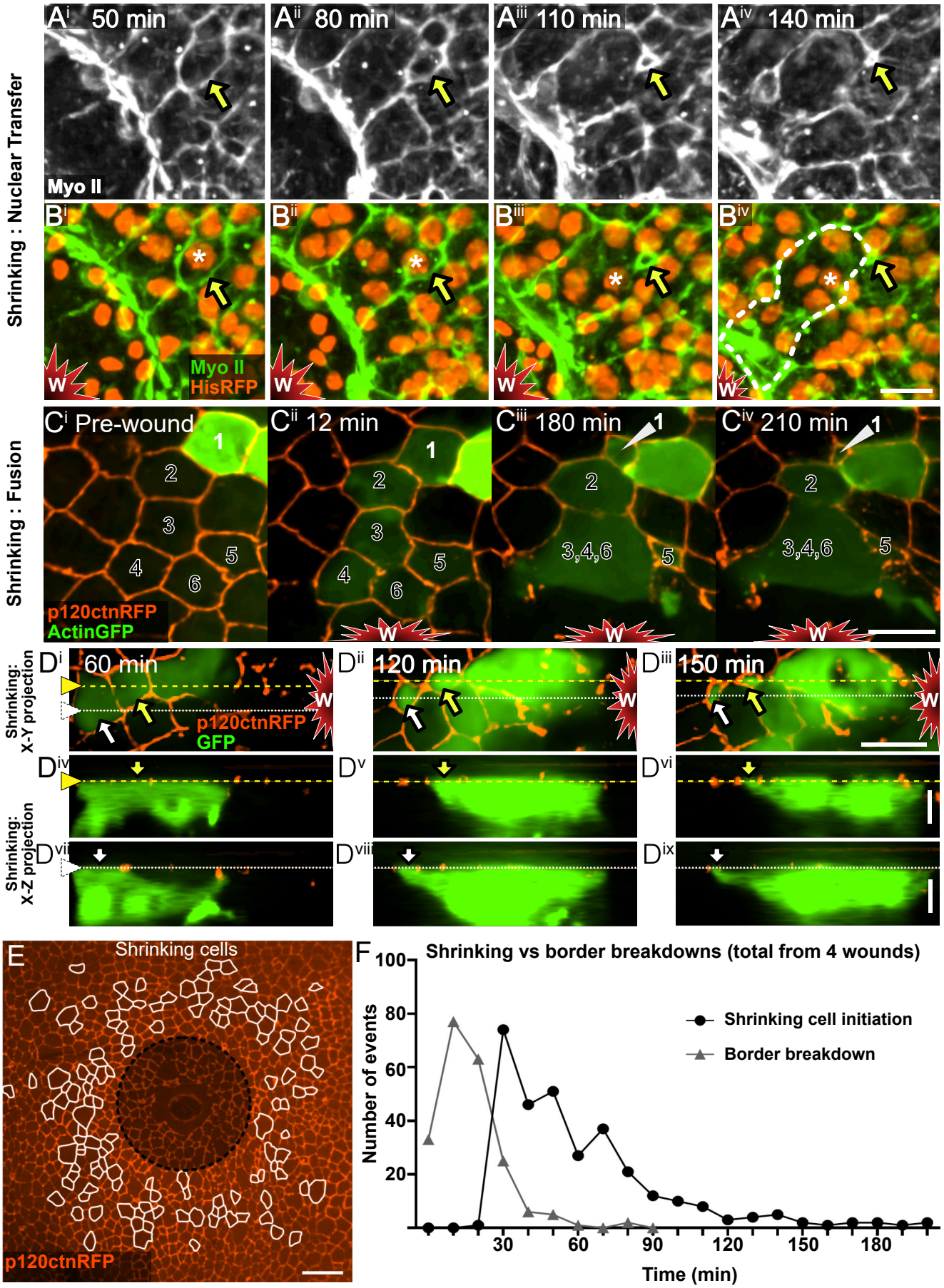
Shrinking : Nuclear Transfer
Ai 50 min
Aii 80 min
Aiii 110 min
Aiv 140 min
Myo II
Bi
Bii
Biii
Biv
Myo II
HisRFP
W
Shrinking : Fusion
Ci Pre-wound
Cii 12 min
Ciii 180 min
Civ 210 min
1
2
3
4
5
6
3,4,6
p120ctnRFP
ActinGFP
Shrinking: X-Y projection
Di 60 min
Dii 120 min
Diii 150 min
p120ctnRFP
GFP
Div
Dv
Dvi
Shrinking: X-Z projection
Dvii
Dviii
Dix
E
Shrinking cells
p120ctnRFP
F
Shrinking vs border breakdowns (total from 4 wounds)
Number of events
Time (min)
Shrinking cell initiation
Border breakdown
100
80
60
40
20
30
60
90
120
150
180

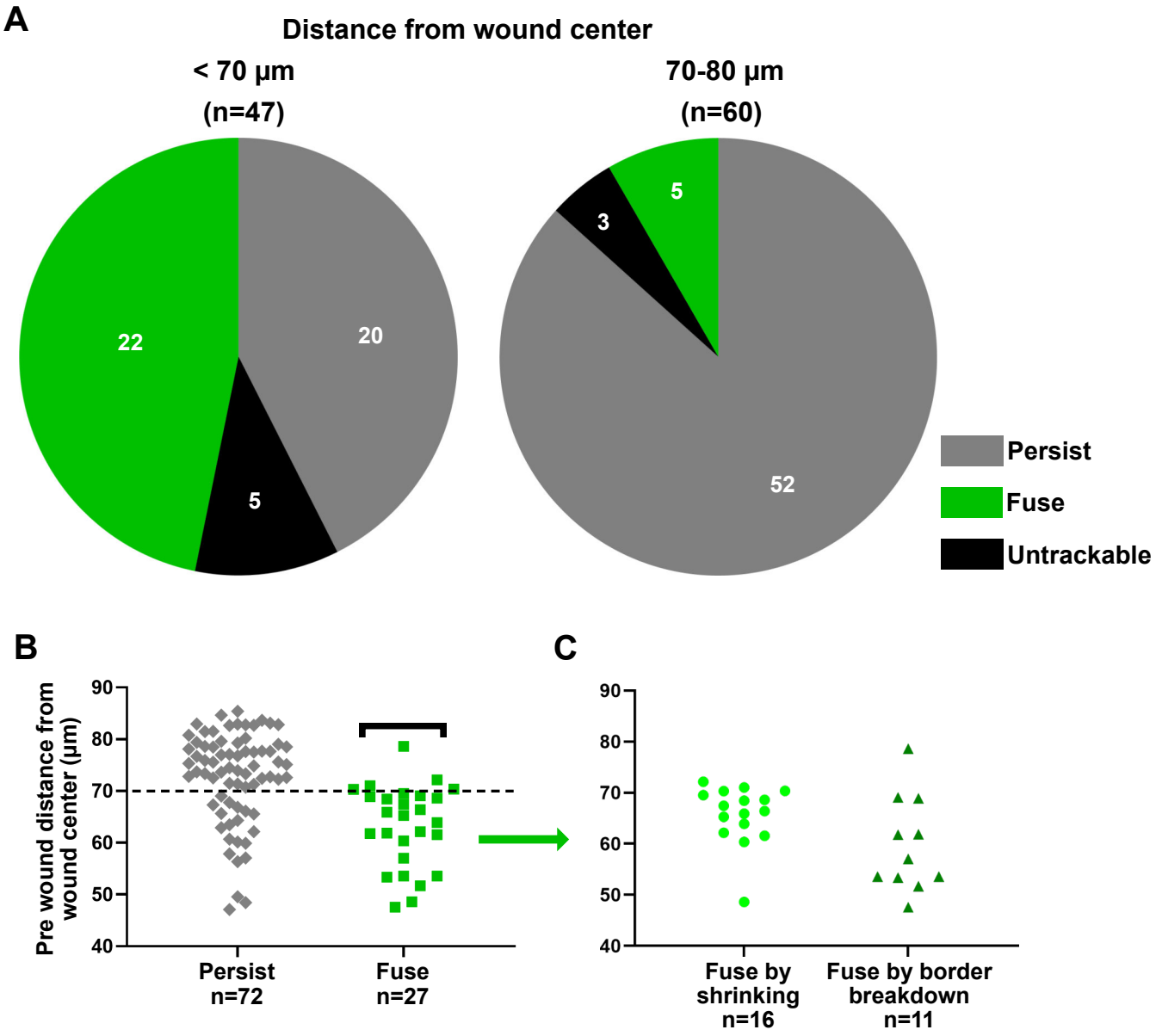
A
Distance from wound center
< 70 µm
(n=47)
70-80 µm
(n=60)
22
20
5
5
3
52
Persist
Fuse
Untrackable
B
Pre wound distance from wound center (µm)
90
80
70
60
50
40
Persist
n=72
Fuse
n=27
C
90
80
70
60
50
40
Fuse by shrinking
n=16
Fuse by border breakdown
n=11

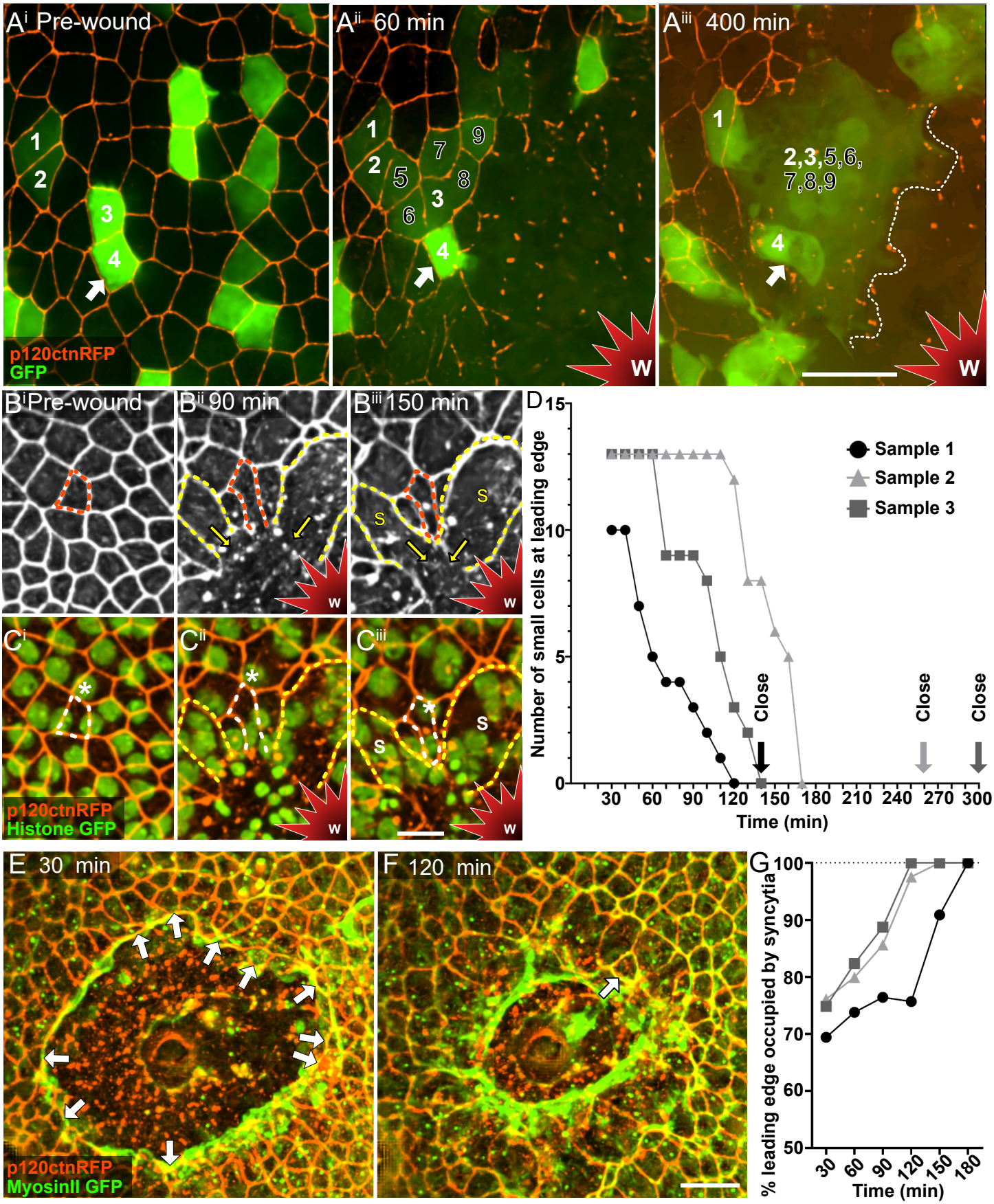
A^i Pre-wound
A^ii 60 min
A^iii 400 min
1
2
3
4
5
6
7
8
9
2,3,5,6,
7,8,9
p120ctnRFP
GFP
W
B^i Pre-wound
B^ii 90 min
B^iii 150 min
S
w
C^i
C^ii
C^iii
*
p120ctnRFP
Histone GFP
D
Number of small cells at leading edge
Time (min)
Sample 1
Sample 2
Sample 3
Close
E 30 min
F 120 min
p120ctnRFP
MyosinII GFP
G
% leading edge occupied by syncytia
Time (min)

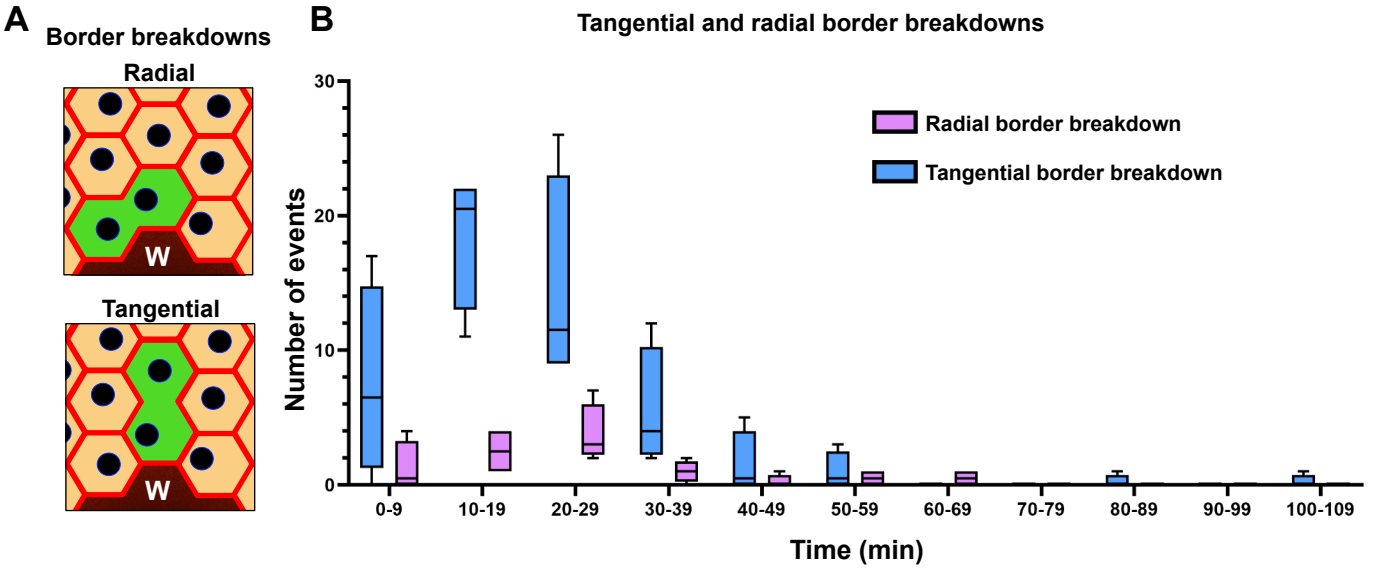

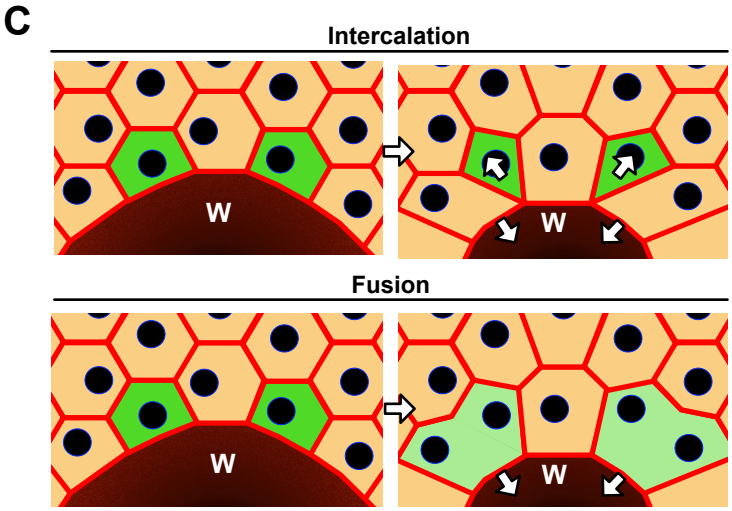

D

	Sample number 1	2	3
Time of closure (min)	140	260	300
# cells lost from leading edge	39	43	42
by fusion	16 (41%)	15 (35%)	7 (17%)
by intercalation	23 (59%)	28 (65%)	35 (83%)

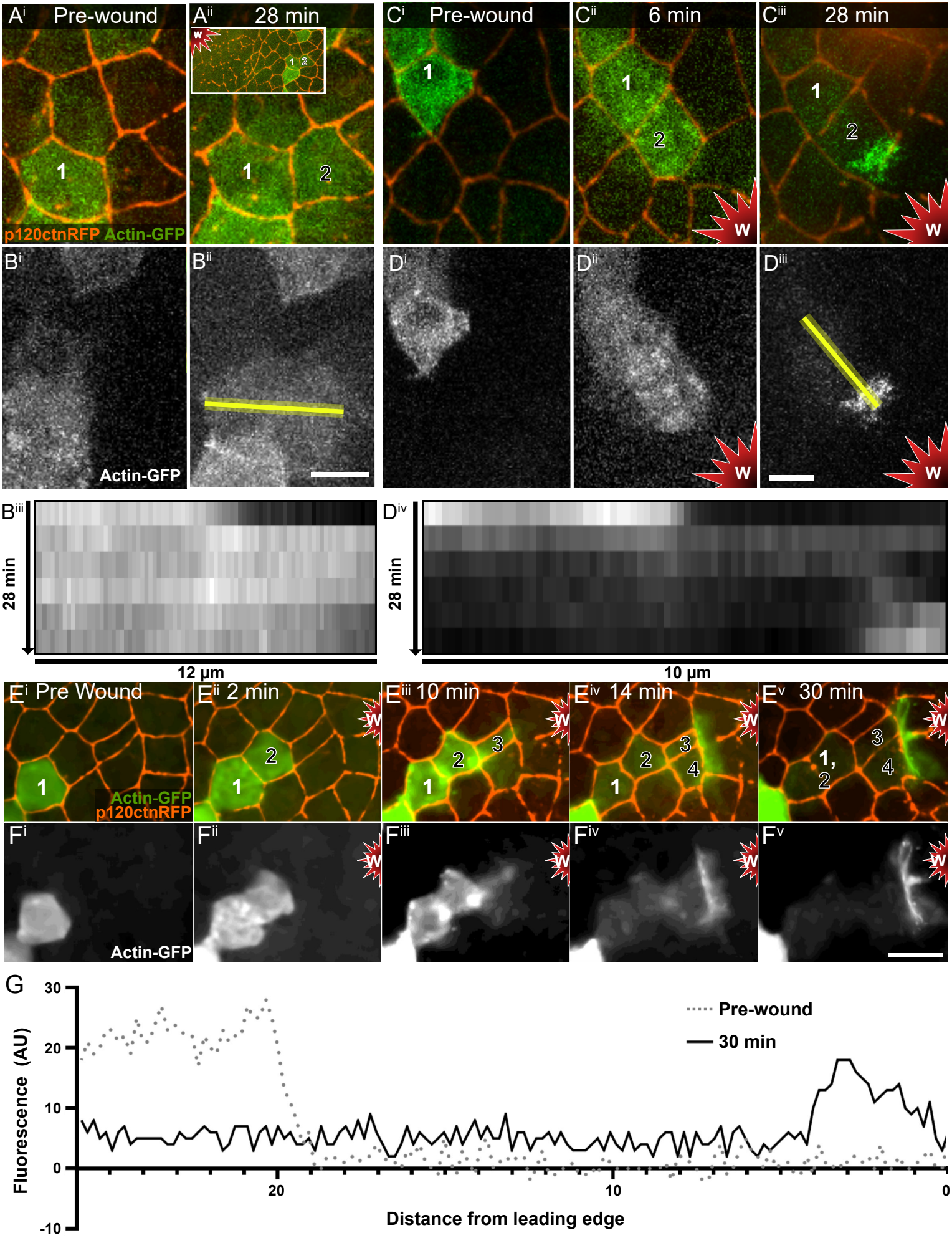
A^i Pre-wound
A^ii 28 min
C^i Pre-wound
C^ii 6 min
C^iii 28 min
p120ctnRFP Actin-GFP
B^i
B^ii
D^i
D^ii
D^iii
Actin-GFP
B^iii
D^iv
28 min
12 µm
10 µm
E^i Pre Wound
E^ii 2 min
E^iii 10 min
E^iv 14 min
E^v 30 min
Actin-GFP
p120ctnRFP
F^i
F^ii
F^iii
F^iv
F^v
G
Fluorescence (AU)
Distance from leading edge
Pre-wound
30 min